

Photoionization cross section calculations for the halogen-like ions Kr^+ and Xe^+

B M McLaughlin^{1,2†} and C P Ballance^{3‡}

¹Centre for Theoretical Atomic, Molecular and Optical Physics, School of Mathematics and Physics, The David Bates Building, 7 College Park, Queen's University Belfast, Belfast BT7 1NN, UK

²Institute for Theoretical Atomic and Molecular Physics, Harvard Smithsonian Center for Astrophysics, Cambridge, MA 02138, USA

³Department of Physics, 206 Allison Laboratory, Auburn University, Auburn, AL 36849, USA

Abstract. Photoionization cross sections calculations on the halogen-like ions; Kr^+ and Xe^+ have been performed for a photon energy range from each ion threshold to 15 eV, using large-scale close-coupling calculations within the Dirac-Coulomb R-matrix approximation. The results from our theoretical work are compared with recent measurements made at the ASTRID merged-beam set-up at the University of Aarhus in Denmark and from the Fourier transform ion cyclotron resonance (FT-ICR) trap method at the SOLEIL synchrotron radiation facility in Saint-Aubin, France [1] and the Advanced Light Source (ALS) [2, 3]. For each of these complex ions our theoretical cross section results over the photon energy range investigated are seen to be in excellent agreement with experiment. Resonance energy positions and quantum defects of the prominent Rydberg resonances series identified in the spectra are compared with experiment for these complex halogen like-ions.

(Figures are in colour only in the online version)

PACS numbers: 32.80.Dz, 32.80.Fb, 33.60-q, 33.60.Fy

Short title: Photoionization cross sections for halogen-like ions

J. Phys. B: At. Mol. Opt. Phys: 25 February 2013

† Corresponding author, E-mail: b.mclaughlin@qub.ac.uk

‡ Corresponding author, E-mail: ballance@physics.auburn.edu

1. Introduction

Most of the known matter in the Universe is in a plasma state and our information about the Universe is carried by photons, which are dispersed and detected for example by the orbiting Chandra X-ray Observatory. While photons travel through stellar atmospheres and planetary nebulae, they are likely to interact with matter and therefore with ions. This makes the study of photoionization of atoms, molecules and their positive ions very important for astrophysicists, helping them to interpret stellar data.

Photoionization cross sections of heavy atomic elements, in low stages of ionization, are currently of interest both experimentally and theoretically and for applications in astrophysics. The data from such processes have many applications in planetary nebulae, where they are of use in identifying weak emission lines of n-capture elements in NGC 3242. For example, the relative abundances of Xe and Kr can be used to determine key physical characteristics of s-process nucleosynthesis, such as the neutron exposure experienced by Fe-peak seed nuclei [4, 7, 5, 6].

Xenon and Krypton ions are also of importance in man-made plasmas such as XUV light sources for semiconductor lithography [8], ion thrusters for space craft propulsion [9], and nuclear fusion plasmas [10]. Xenon and Krypton ions have also been detected in cosmic objects, e.g., in several planetary nebulae and in the ejected envelopes of low- and intermediate-mass stars [13, 11, 7, 12, 5]. For a profound understanding of these plasmas accurate cross sections are required for ionization and recombination processes that govern the charge balance of ions in plasmas. Krypton and xenon ions are of particular importance in tokamak plasmas. Injection of high-Z gases, essentially Kr and Xe, has been proposed as a technique to mitigate disruption [14, 15], i.e. the uncontrolled and sudden loss of tokamak plasma current and energy. Disruption can produce severe damage on the vessel wall. The situation becomes more critical for large machines such as ITER (International Thermonuclear Experimental Reactor), where incident-loading energy may reach several GW m^{-2} [16, 17]. After injection of the gases, highly-charged Kr and Xe ions are dominant in the core of the plasma, and low-charged and singly-charged ions are abundant near the edge.

Over the past decade, experimentally, photoionization data on ionic targets have been obtained using mainly two techniques: DLPP (dual laser produced plasma) and merged beam in synchrotron radiation facilities. While the former technique measures photoabsorption spectra [18], the latter provides absolute single and multiple photoionization cross sections [19, 20]. As indicated by Bizau and co-workers [1] in recent studies on Kr^+ and Xe^+ ions, in the valence region, only the K-shell photoionization of the Kr^+ ion has been reported on [21]. The bulk of the studies on the Xe^+ ion have focused primarily on the region of 4d inner-shell excitation and ionization using the merged-beam technique [22, 23, 24, 25, 26]. The recent work on Xe^+ of Bizau and co-workers [1] together with the ongoing high resolution studies at the ALS [2, 3], in the threshold region, make it pertinent to have suitable theoretical results available to compare with. As pointed out in the recent work of Bizau and co-workers [1], no studies using the above experimental techniques have been published on the Kr^+ ion or on the Xe^+ ion in any other energy range and, in particular, close to the thresholds, where strong resonance features dominate the respective cross sections. Furthermore, no theoretical results on the photoionization processes are available for these ions outside the region of 4d inner-shell excitation in the Xe^+ ion. In order to address these limitations, particularly for astrophysical applications, we

have carried out large scale photoionization cross section calculations in the threshold region for both singly ionized ions of krypton and xenon. Where possible we have benchmarked our theoretical work with the available experimental data in order to provide confidence in our work for applications.

The layout of this paper is as follows. Section 2 presents a brief outline of the theoretical work. Section 3 details the results obtained. Section 4 presents a discussion and a comparison of the results obtained between experiment and theory. Finally in section 5 conclusions are drawn from the present investigation.

2. Theory

Recent modifications to the Dirac-Atomic-R-matrix-Codes (DARC) [27] has now made it feasible to study photoionization of heavy complex systems of prime interest to astrophysics and plasma applications by including hundreds of target levels in the close-coupling calculations. This enables photoionization calculations on complex ions such as singly ionized ions of Krypton and Xenon, the focus of the current investigation to be carried out at the same degree of accuracy as those for electron impact excitation. Such extensions to the DARC codes have allowed us recently to address the complex problem of trans-iron element single photon ionization of Se^+ ions. In the present study we apply this suite of DARC codes to calculate detailed photoionization (PI) cross sections on the halogen-like ions, Kr^+ and Xe^+ . Recent experimental measurements [1] have been made on these systems but limited theoretical work is available to compare with. Photoionization cross sections on these halogen-like ions are performed for the ground and the excited metastable levels associated with the ns^2np^5 configuration ($n=4$ and 5 respectively for Kr^+ and Xe^+ ions) in order to benchmark our theoretical results with recent high resolution experimental measurements [1].

For both the ground and metastable initial states, the outer region electron-ion collision problem for each ion was solved (in the resonance region below and between all thresholds) using a suitably chosen fine energy mesh of 5×10^{-8} Rydbergs ($\approx 0.68 \mu\text{eV}$) to fully resolve all the extremely narrow resonance structure in the appropriate photoionization cross sections. The jj-coupled Hamiltonian diagonal matrices were adjusted so that the theoretical term energies matched the recommended experimental values of NIST [28]. We note that this energy adjustment ensures better positioning of resonances relative to all thresholds included in the calculation. In the energy region considered here we can see from Tables 1 and 2 the shift to the 1D_2 and 1S_0 thresholds is minimal. For this reason in Table 3 - 5 we only include experimental series limits.

In order to compare directly with the available experimental measurements for each of these ions, we have convoluted the theoretical PI cross sections with a gaussian function of the appropriate full width half maximum (FWHM) and statistically averaged the results for the ground and metastable states.

2.1. Kr^+

Photoionization (PI) cross section calculations on the Kr^+ complex were carried out retaining 326-levels in our close-coupling calculations with the Dirac-Atomic-R-matrix-Codes (DARC). In R-matrix theory, all photoionization cross section calculations require the generation of atomic orbitals based primarily on the atomic structure of the residual ion. The present theoretical work for the photoionization of the Kr^+ ion employs relativistic atomic orbitals up to $n=4$ generated for the residual

Table 1. Comparison of the theoretical energies using the GRASP code from the 326-level model, relative energies are in Rydbergs. A sample of the first 8 levels of the Kr III ion are compared with the NIST [28] tabulated values.

Level	Configuration	Term ^a	Energy NIST	Energy GRASP	$\Delta(\%)^b$
1	4s ² 4p ⁴	³ P ₂	0.000000	0.000000	0.0
2	4s ² 4p ⁴	³ P ₁	0.041448	0.040837	0.8
3	4s ² 4p ⁴	³ P ₀	0.048415	0.048845	0.9
4	4s ² 4p ⁴	¹ D ₂	0.133449	0.152130	14.0
5	4s ² 4p ⁴	¹ S ₀	0.301443	0.318538	5.7
6	4s ¹ 4p ⁵	³ P ₂ ^o	1.0564404	1.230028	16.4
7	4s ¹ 4p ⁵	³ P ₁ ^o	1.0878727	1.263533	16.1
8	4s ¹ 4p ⁵	³ P ₀ ^o	1.1075809	1.282909	15.8

^a $2S+1L_J^\pi$ ^b GRASP, absolute percentage difference relative to NIST values**Table 2.** Comparison of the theoretical energies using the GRASP code from the 326-level model, relative energies are in Rydbergs. A sample of the lowest 8 levels of the Xe III ion are compared with the NIST [28] tabulated values.

Level	Configuration	Term ^a	Energy NIST	Energy GRASP	$\Delta(\%)^b$
1	5s ² 5p ⁴	³ P ₂	0.000000	0.000000	0.0
2	5s ² 5p ⁴	³ P ₁	0.074087	0.074275	0.3
3	5s ² 5p ⁴	³ P ₀	0.089253	0.082014	8.1
4	5s ² 5p ⁴	¹ D ₂	0.155815	0.173148	11.1
5	5s ² 5p ⁴	¹ S ₀	0.328994	0.334735	1.7
6	5s ¹ 5p ⁵	³ P ₂ ^o	0.895434	0.904921	2.2
7	5s ¹ 5p ⁵	³ P ₁ ^o	0.943783	0.953095	1.0
8	5s ¹ 5p ⁵	³ P ₀ ^o	0.987210	0.987768	0.1

^a $2S+1L_J^\pi$ ^b GRASP, absolute percentage difference relative to NIST values

Kr²⁺ ion, which were calculated using the extended-optimal-level (EOL) procedure within the GRASP structure code [29, 30, 31]. The 1s-4s, 2p-4p and 3d-4d orbitals were obtained from an EOL calculation on the lowest 14 levels associated with the 4s²4p⁴, 4s4p⁵ and 4s²4p²4d² configurations where the remaining four configurations; 4s²4p³4d, 4s²4p²4d², 4s4p⁴4d and 4p⁴4d² were included in the calculation. Table 1 illustrates a sample of our target energy levels for the residual Kr III ion compared to the NIST tabulation [28] for the lowest 8 levels associated with the 4s²4p⁴ and 4s4p⁵ configurations.

Photoionization cross section calculations for this complex trans-iron element included all 326 levels arising from the seven configurations: 4s²4p⁴, 4s4p⁵, 4s²4p³4d, 4s²4p²4d², 4p⁶, 4s4p⁴4d and 4p⁴4d² in the close-coupling expansion. PI cross section calculations with this 336-level model were performed in the Dirac-Coulomb approximation using the DARC codes.

The R-matrix boundary radius of 7.44 Bohr radii was sufficient to envelop the radial extent of all the atomic orbitals of the residual Kr²⁺ ion. A basis of 16 continuum orbitals was sufficient to span the incident experimental photon energy

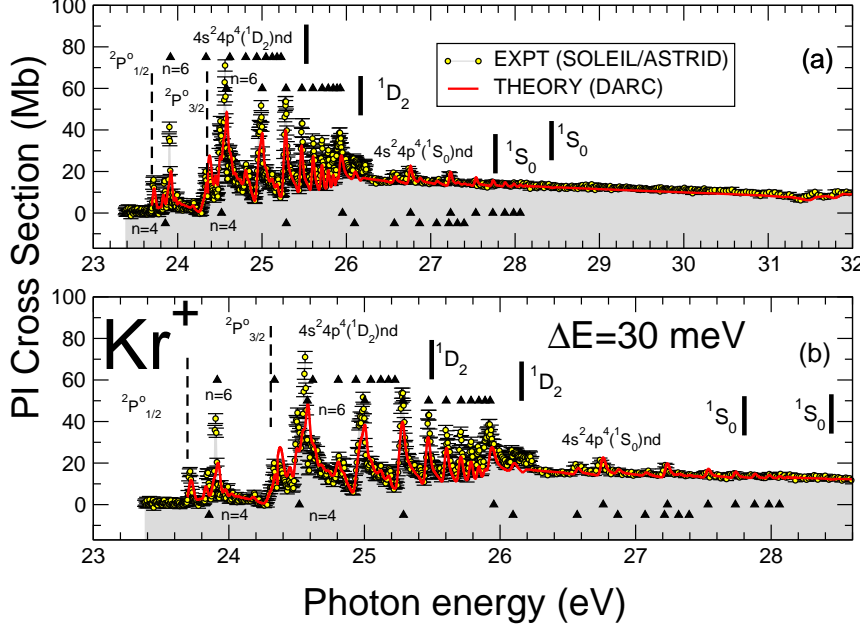


Figure 1. Theoretical cross sections for photoionization (PI) of Halogen-like Kr^+ ions. (a) The 326-state jj -coupling R-matrix calculations were carried out for ground-state and metastable-state parent ions using the recently developed DARC suite of codes. The theoretical cross sections (solid line) were convoluted at 30 meV FWHM and statistically averaged in order to compare directly with the recent experimental results [1] for the energy range threshold. The prominent Rydberg resonance series $4s^2 4p^4 (1D_2, 1S_0)nd$ converging to the Kr^{2+} ($1D_2$ and $1S_0$) thresholds (b) are tabulated in Table 1 and 2.

range from threshold up to 40 eV. The 326-state model produced a maximum of 1511 coupled channels in our scattering work with Hamiltonian matrices of dimension of the order of 24,354 by 24,354 in size. Due to dipole selection rules, for total ground state photoionization we need only to consider the bound-free dipole matrices, $2J^\pi = 3^o \rightarrow 2J^\pi = 1^e, 3^e, 5^e$ whereas for the excited metastable states only the $2J^\pi = 1^o \rightarrow 2J^\pi = 1^e, 3^e$ ones are required.

2.2. Xe^+

Similarly for photoionization cross section calculations on the Xe^+ system we retained 326 levels of the residual Xe^{2+} ion in our close-coupling calculations performed with the Dirac-Atomic-R-matrix-Codes (DARC). Analogous PI calculations on the Kr^+ case, were made similarly for the Xe^+ ion. For the Xe^+ case we have employed relativistic $n=5$ atomic orbitals generated for the residual Xe^{2+} ion, which were obtained using the energy-average-level (EAL) procedure within the GRASP structure code on the

Table 3. Principal quantum number (n), resonance energies E (eV) and quantum defect (μ) from experimental measurements of Kr^+ [1] compared with present theoretical estimates from the QB method. The Rydberg series $4s^2 4p^4(^1D_2)nd$ originating from the $^2P_{3/2}^\circ$ ground state and the $^2P_{1/2}^\circ$ metastable state of Kr^+ due to $4p \rightarrow nd$ transitions are tabulated .

Initial Kr^+ state $4s^2 4p^5 (^2P_{3/2}^\circ)$			Initial Kr^+ state $4s^2 4p^5 (^2P_{3/2}^\circ)$		
Rydberg Series $4s^2 4p^4(^1D_2)nd$			Rydberg Series $4s^2 4p^4(^1D_2)nd$		
n	E (eV)	μ	n	E (eV)	μ
[Theory]			[Experiment]		
6	24.579	0.16	6	24.562	0.19
7	25.002	0.19	7	24.989	0.23
8	25.284	0.19	8	25.280	0.20
9	25.473	0.20	9	25.475	0.19
10	25.603	0.25	10	25.605	0.23
11	25.713	0.16	11	25.710	0.19
12	25.786	0.18	12	25.785	0.19
13	25.844	0.19	13	25.842	0.23
14	25.890	0.19	—	—	—
15	25.927	0.19	—	—	—
.	—
∞	26.176 [†]		∞	26.176 [†]	

Initial Kr^+ state $4s^2 4p^5 (^2P_{1/2}^\circ)$			Initial Kr^+ state $4s^2 4p^5 (^2P_{1/2}^\circ)$		
Rydberg Series $4s^2 4p^4(^1D_2)nd$			Rydberg Series $4s^2 4p^4(^1D_2)nd$		
n	E (eV)	μ	n	E (eV)	μ
[Theory]			[Experiment]		
6	23.914	0.16	6	23.902	0.18
7	24.336	0.19	7	24.334	0.20
8	24.619	0.19	8	24.613	0.21
9	24.807	0.20	9	24.811	0.17
10	24.937	0.25	10	24.989	0.23
11	25.047	0.16	11	25.047	0.15
12	25.121	0.18	12	25.119	0.20
13	25.178	0.18	13	25.180	0.15
14	25.225	0.19	—	—	—
15	25.262	0.19	—	—	—
.	.	—	.	.	—
∞	25.510 [†]		∞	25.510 [†]	

[†]NIST tabulations [28]

Table 4. Principal quantum number (n), resonance energies E (eV) and quantum defect (μ) from experimental measurements of Kr^+ [1] compared with present theoretical estimates from the QB method. The Rydberg series $4s^2 4p^4(^1S_0) nd$ originating from the $^2P_{3/2}^o$ ground state and $^2P_{1/2}^o$ metastable state of Kr^+ due to $4p \rightarrow nd$ transitions are tabulated.

Initial Kr^+ state $4s^2 4p^5 (^2P_{3/2}^o)$			Initial Kr^+ state $4s^2 4p^5 (^2P_{3/2}^o)$		
Rydberg Series $4s^2 4p^4(^1S_0) nd$			Rydberg Series $4s^2 4p^4(^1S_0) nd$		
n	E (eV)	μ	n	E (eV)	μ
[Theory]			[Experiment]		
4	24.520	0.28	4	24.501	0.29
5	25.954	0.34	5	25.910	0.38
6	26.761	0.34	6	26.740	0.38
7	27.235	0.34	7	27.230	0.35
8	27.534	0.34	8	27.530	0.38
9	27.736	0.34	9	—	—
10	27.878	0.34	10	—	—
11	27.983	0.33	11	—	—
12	28.061	0.33	12	—	—
·	·	·	·	·	·
∞	28.461 [†]		∞	28.461 [†]	

Initial Kr^+ state $4s^2 4p^5 (^2P_{1/2}^o)$			Initial Kr^+ state $4s^2 4p^5 (^2P_{1/2}^o)$		
Rydberg Series $4s^2 4p^4(^1S_0) nd$			Rydberg Series $4s^2 4p^4(^1S_0) nd$		
n	E (eV)	μ	n	E (eV)	μ
[Theory]			[Experiment]		
4	23.854	0.28	4	23.845	0.29
5	25.288	0.34	5	25.280	0.20
6	26.096	0.34	6	26.100	0.33
7	26.569	0.34	7	26.580	0.31
8	26.868	0.34	8	—	—
9	27.070	0.34	9	—	—
10	27.213	0.34	10	—	—
11	27.317	0.33	11	—	—
12	27.395	0.33	12	—	—
·	·	·	·	·	·
∞	27.795 [†]		∞	27.795 [†]	

[†]NIST tabulations [28]

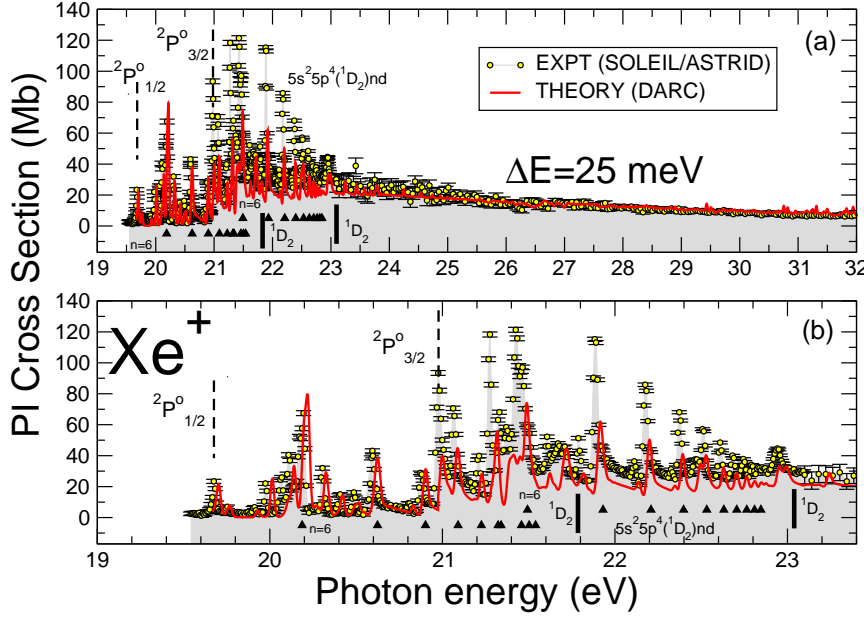


Figure 2. Theoretical cross sections for photoionization (PI) of Halogen-like Xe^+ ions. (a) The 326-state jj -coupling R-matrix calculations were carried out for ground-state and metastable-state parent ions using the recently developed DARC suite of codes. The theoretical cross sections (solid line) were convoluted at 25 meV FWHM and statistically averaged. The experiment data [1] was normalized to theory at 28 eV in order to have a direct comparison. The prominent Rydberg resonance series $5s^2 5p^4 ({}^1D_2) nd$ converging to the $\text{Xe}^{2+} ({}^1D_2)$ threshold (b) are tabulated in Table 5.

fourteen lowest levels associated with the $5s^2 5p^4$, $5s 5p^5$ and $5s^2 5p^3 5d^2$ configurations. Table 2 gives a sample of our results for the Xe III ion for the energies of the lowest eight levels associated with the $5s^2 5p^4$ and $5s 5p^5$ configurations compared with the NIST [28] tabulations. Here again for the photoionization cross section calculations on this complex trans-iron system we included all 326 levels arising from the seven configurations: $5s^2 5p^4$, $5s 5p^5$, $5s^2 5p^3 5d$, $5s^2 5p^2 5d^2$, $5p^6$, $5s 5p^4 5d$ and $5p^4 5d^2$ in the close-coupling expansion. PI cross section calculations with this 326-level model were then carried out in the Dirac-Coulomb approximation using the DARC codes for photon energies up to about 15 eV above the ion threshold.

3. Results

Figures 1 and 2 presents our theoretical results from the 326-level model using the DARC suite of codes. In order to compare directly with the experimental results of Bizau and co-workers [1] we have statistically averaged the results from the ground

Table 5. Principal quantum number (n), resonance energies E (eV) and quantum defect (μ) from experimental measurements of Xe^+ [1] compared with present theoretical estimates from the QB method. The Rydberg series $5s^25p^4(^1D_2)nd$ originating from the $^2P_{3/2}^\circ$ ground state and the $^2P_{1/2}^\circ$ metastable state of Xe^+ due to $5p \rightarrow nd$ transitions are tabulated.

Initial Xe^+ state $5s^25p^5(^2P_{3/2}^\circ)$				Initial Xe^+ state $5s^25p^5(^2P_{3/2}^\circ)$			
Rydberg Series $5s^25p^4(^1D_2)nd$				Rydberg Series $5s^25p^4(^1D_2)nd$			
n	E (eV)	μ		n	E (eV)	μ	
[Theory]				[Experiment]			
6	21.493	0.17		6	21.425	0.29	
7	21.931	0.16		7	21.886	0.29	
8	22.209	0.16		8	22.177	0.30	
9	22.398	0.17		9	22.375	0.31	
10	22.532	0.17		10	22.510	0.35	
11	22.631	0.17		11	22.610	0.41	
12	22.706	0.17		12	22.683	0.51	
13	22.764	0.18		13	22.747	0.49	
14	22.809	0.20		—	—	—	
15	22.846	0.20		—	—	—	
·	·	·	—	·	·	·	—
∞	23.095 [†]			∞	23.095 [†]		

Initial Xe^+ state $5s^25p^5(^2P_{1/2}^\circ)$				Initial Xe^+ state $5s^25p^5(^2P_{1/2}^\circ)$			
Rydberg Series $5s^25p^4(^1D_2)nd$				Rydberg Series $5s^25p^4(^1D_2)nd$			
n	E (eV)	μ		n	E (eV)	μ	
[Theory]				[Experiment]			
6	20.187	0.17		6	20.195	0.16	
7	20.624	0.16		7	20.594	0.25	
8	20.902	0.16		8	20.876	0.28	
9	21.091	0.16		9	21.062	0.34	
10	21.226	0.17		10	21.210	0.30	
11	21.323	0.17		—	—	—	
12	21.340	0.17		—	—	—	
13	21.458	0.18		—	—	—	
14	21.503	0.20		—	—	—	
15	21.540	0.20		—	—	—	
·	·	·		·	·	·	—
∞	21.789 [†]			∞	21.789 [†]		

[†]NIST tabulations [28]

and metastable levels and convoluted respective cross sections with a Gaussian of 30 meV FWHM for Kr^+ ions and 25 meV for Xe^+ ions. In the near threshold region (cf figures 1 b and 2 b) we see clearly (from a comparison of the theoretical and experimental results of Bizau et al [1]) that the rich and complex resonance structure is better reproduced by the DARC calculations for Kr^+ than for Xe^+ , which could be due to the limited resolution in those experiments. Figure 3 shows a comparison with recent ALS measurements for Xe^+ ions in the near threshold region taken at the Advanced Light Source (ALS) at an extremely high resolution of 4 meV [2]. Here we see that the experimental PI cross sections (apart from the region of the $n=14$ member of the $5s^25p^4$ (3P_1) nd series) are reproduced by our DARC calculations.

The multi-channel R-matrix eigenphase derivative (QB) technique (applicable to atomic and molecular complexes) of Berrington and co-workers [32, 33, 34] modified to cater for jj-coupling was used to determine the resonance parameters of the prominent series. The resonance width Γ was determined from the inverse of the energy derivative of the eigenphase sum δ at the resonance energy E_r via

$$\Gamma = 2 \left[\frac{d\delta}{dE} \right]_{E=E_r}^{-1}. \quad (1)$$

The results for all the resonance parameters determined from the QB method are presented in Tables 3 and 4 for Kr^+ ions and compared with the available experimentally determined ones. Table 5 give similar results for the corresponding Xe^+ ion.

4. Discussion

The hypothesis of statistical population is very reasonable since the life time is huge (0.34 seconds for the case of Kr^+) if compared to the beam transport times. Note also that the excited $^2P_{1/2}^o$ metastable Kr^+ ions produced either in an ion source or ion trap rarely collide with surfaces or residual gas before photoionization takes place. As a result, statistical population of the ions seems consistent with their measurements both using an ion source and an ion trap without delay[1]. For the case of Kr^+ ions studied here resonance positions and quantum defects are in excellent agreement with the available experimental measurements as can be seen from Tables 3 and 4. The magnitude of the absolute cross sections are also in excellent agreement with experimental values as illustrated in figure 1.

For Xe^+ ions the difference in the resolution between the Bizau and co-workers [1] (25 meV) and current Advanced Light Source (ALS) measurements (2.2 meV) [2] and that taken at 4 meV shown in figure 3 [3] is over a factor of ten better. Bizau and co-workers noted that, given their poor resolution, they do not attempt to obtain more detailed spectroscopic information: "Considering the moderate energy resolution chosen in this work to compensate for the low density of target ions, we have not attempted a detailed identification of the observed structures, which are most of the time composed of several unresolved lines." In the near threshold region we do not fully reproduce the resonance strengths in the experimental data of Bizau and co-workers [1] which could be due to the limited resolution in those experiments. We also note here there is a discrepancy in the quantum defects for the Rydberg series in Xe^+ as given in Table 5 with the experimental values of Bizau and co-workers [1]. The recent high resolution measurements (4 meV) see figure 3 made at the ALS by Muller and co-workers [3] have made possible spectroscopic studies of the Xe^+ PI spectrum in

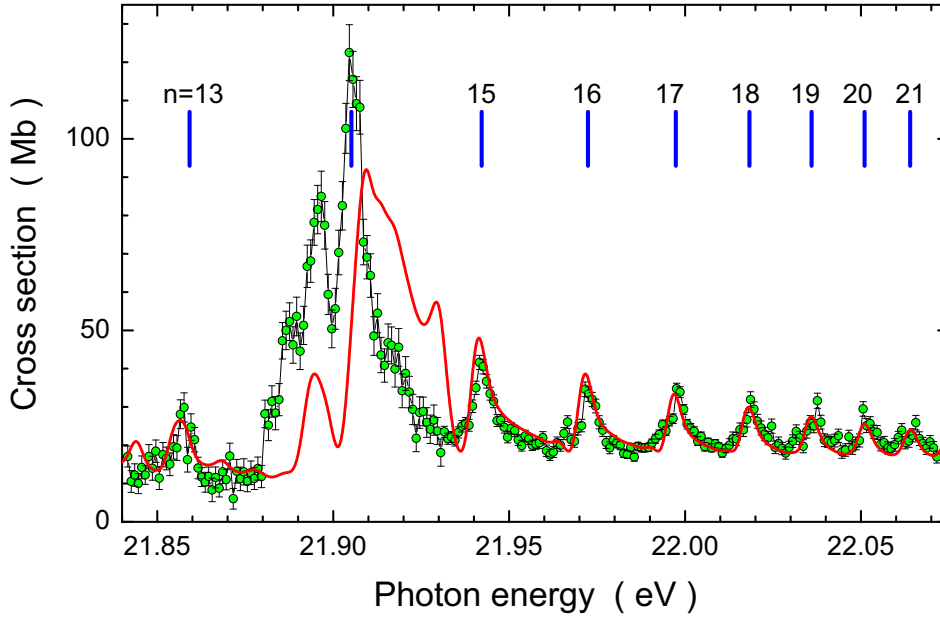


Figure 3. Xe^+ ALS experimental PI cross section data (green circles) for photon energies ranging from 21.84 eV - 22.08 eV at a photon energy resolution of 4 meV. Results are compared with theoretical results from a 326-level Dirac-Coulomb R-matrix calculation (red line) convoluted with a FWHM Gaussian of 4 meV and statistically averaged over the ground and metastable states to simulate the experimental measurements. The bars mark the energies of the $[5s^2 5p^4 ({}^3P_1) nd]$ resonances obtained with a quantum defect of 0.16. [2, 3]

the near threshold region producing an average quantum defect for the $5s^2 5p^4 ({}^3P_1) nd$ Rydberg series of 0.16 which are comparable values to our DARC estimates for the $5s^2 5p^4 ({}^1D_2) nd$ series in Table 5 [2, 3]. For Xe^+ ions a more stringent test with recent extremely high resolution experimental measurements made at the ALS at 4 meV indicate (in the near threshold region, apart from the $n=14$ member of the Rydberg series) very good agreement giving us confidence in our theoretical results.

5. Conclusions

State-of-the-art theoretical methods were used to investigate photons interacting with the halogen-like ions, Kr^+ and Xe^+ , in the energy region extending to about 15 eV beyond the ionization threshold. Given the complexity of these halogen-like ions, throughout the energy region investigated the agreement (on the photon-energy scale and on the absolute PI cross-section scale) is better for Kr^+ ions than for Xe^+ ions with the recent experimental measurements of Bizau and co-workers [1] and our DARC calculations. However our DARC calculations in the near threshold region are seen to reproduce most of the recent extremely high resolution ALS measurements on Xe^+ ions [2, 3]. It is seen that the photoionization cross section exhibits a wealth of resonances which theory is able to mostly reproduce. The prominent members of the Rydberg series are analyzed and compared with experiment. We point out that the strength of the present study is the benchmarking of our theoretical work

with the available experimental data. Such detailed comparison between theory and experiment strengthens the validity of our results giving confidence in their use for astrophysical applications.

The photoionization cross-sections from the present study are suitable to be included into state-of-the-art photoionization modelling codes Cloudy and XSTAR [35, 36] that are used to numerically simulate the thermal and ionization structure of ionized astrophysical nebulae.

Acknowledgments

C P Ballance was supported by US Department of Energy (DoE) grants through Auburn University. B M McLaughlin acknowledges support by the US National Science Foundation through a grant to ITAMP at the Harvard-Smithsonian Center for Astrophysics. We thank Dr Jean-Marc Bizau for providing us with the recent ASTRID/SOLEIL experimental data on these ions and Professor Alfred Mueller for the ALS experimental data. The computational work was carried out at the National Energy Research Scientific Computing Center in Oakland, CA, USA and on the Tera-grid at the National Institute for Computational Sciences (NICS) in Knoxville, TN, USA.

- [1] Bizau J M *et al* 2011 *J. Phys. B: At. Mol. Opt. Phys.* **44** 055205
- [2] Müller A 2012 *private communication*.
- [3] Aguilier A, Alna'washi G, Bilodeau R C, Carr A, Esteves D, Kilcoyne A L D, Müller A M, Phaneuf R A, Red E, Schippers S, Sterling N C, Ballance C P and McLaughlin B M 2012 XXVII International Conference on Photonic, Electronic and Atomic Collisions *J. Phys. Conf. Series* vol **XX** ed McCann J F *et al* (Bristol, UK: Institute of Physics (IOP)) p in press
- [4] Sharpee B, Zhang Y, Williams R, Pellegrini E, Cavagnolo K, Baldwin J A, Phillips M and Liu X W 2007 *Astrophys. J.* **659** 1265
- [5] Sterling N C, Dinerstein H L, Hwang S, Redfield S, Aguilar A, Witthoeft M C, Esteves D, Kilcoyne A L D, Bautista M, Phaneuf R A, Bilodeau R, Ballance C P, McLaughlin B M and Norrington P H 2009 *Pub. Astron. Soc. Aust. (PASA)* **26** 339
- [6] Karakas A I, van Raai M A, Lugaro M, Sterling N C and Dinerstein H L 2009 *Astrophys. J.* **690** 1130
- [7] Sterling N C, Dinerstein H L and Kallman T R 2007 *Astrophys. J. Suppl. Ser.* **169** 37
- [8] Kieft E R *et al* 2005 *Phys. Rev. E* **71** 036402
- [9] Lerner E J 2000 *The Industrial Physicist* **6** 16
- [10] Skinner C H 1997 *Phys. Scr.* **T134** 014022
- [11] Sterling N C and Dinerstein H L 2005 An Infrared Survey of Neutron-Capture Elements in Planetary Nebulae *Cosmic Abundances as Records of Stellar Evolution and Nucleosynthesis (ASP Conf. Series* vol **336**) ed Barnes III T G and Bash F N (San Francisco, CA: Astronomical Society of the Pacific) p 367
- [12] Sterling N C and Dinerstein H L 2008 *Astrophys. J. Suppl. Ser.* **174** 157
- [13] Yüce K, Castelli F and Hubrig S 2011 *Astron. Astrophys.* **528** A37
- [14] Riccardo V *et al* 2002 *Plasma Phys. Control. Fusion* **44** 905
- [15] Nishida V *et al* 2002 *Nucl. Fusion* **42** 1197
- [16] Federici G *et al* 2002 *Nucl. Fusion* **41** 1967
- [17] ITER Physics Basis 1999 *Nucl. Fusion* **39** 2137
- [18] Carroll P K and Costello J 1986 *Phys. Rev. Lett.* **57** 1581
- [19] West J B 2001 *J. Phys. B: At. Mol. Opt. Phys.* **34** R45
- [20] Kjeldsen H 2006 *J. Phys. B: At. Mol. Opt. Phys.* **39** R325
- [21] Southworth S *et al* 2006 *Phys. Rev. A.* **76** 043421
- [22] Sano M *et al* 1996 *J. Phys. B: At. Mol. Opt. Phys.* **29** 5305
- [23] Koizumi T *et al* 1997 *Phys. Scr.* **T73** 131
- [24] Andersen P *et al* 2001 *J. Phys. B: At. Mol. Opt. Phys.* **34** 2009
- [25] Itoh Y *et al* 2001 *J. Phys. B: At. Mol. Opt. Phys.* **34** 3493
- [26] Gottwald A, Gert C and Richter M 1999 *Phys. Rev. Lett.* **82** 2068
- [27] Fivet V, Bautista M A and Ballance C P 2012 *J. Phys. B: At. Mol. Opt. Phys.* **45** 035201

- [28] Ralchenko Y, Kramida A E, Reader J, and NIST ASD Team (2011), NIST Atomic Spectra Database (version 4.0.1), National Institute of Standards and Technology, Gaithersburg, MD, USA, URL <http://physics.nist.gov/asd3>
- [29] Dyall K G, Grant I P, Johnson C T and Plummer E P 1989 *Comput. Phys. Commun.* **55** 425
- [30] Parpia F, Froese Fischer C and Grant I P 2006 *Comput. Phys. Commun.* **94** 249
- [31] Grant I P 2007 *Quantum Theory of Atoms and Molecules: Theory and Computation* (New York, USA: Springer)
- [32] Quigley L and Berrington K A 1996 *J. Phys. B: At. Mol. Phys.* **29** 4529
- [33] Quigley L, Berrington K A and Pelan J 1998 *Comput. Phys. Commun.* **114** 225
- [34] Ballance C P, Berrington K A and McLaughlin B M 1999 *Phys. Rev. A* **60** R4217
- [35] Ferland G J, Korista K T, Verner D A, Ferguson J W, Kingdon J B and Verner E M 1998 *PASP* **110** 761
- [36] Kallman T and Bautista M 2001 *Astrophys. J. Suppl. Ser.* **133** 221